Parabolic Deformable Mirror Testbed for the ExoSpec Project

Hari B. Subedi[a], Roser Juanola-Parramon [a,b], Tyler D. Groff[a], and John Hagopian[a,c]

[a]NASA Goddard Space Flight Center, Greenbelt MD, 20771
[b] UMBC, MD
[c] Lambda Consulting, MD

ABSTRACT

The ExoSpec Project is a NASA Headquarters directed work package that links four different tasks at Goddard Space Flight Center to enable future missions to more efficiently characterize directly imaged exoplanets. One of the tasks is the development of parabolic deformable mirrors to improve on the current state-of-the-art wavefront sensing and control implementations, which are baselined to have two flat deformable mirrors (DMs) with high actuator count. To effectively control both amplitude and phase aberrations, the flat DMs need to have a large separation, which poses packaging challenges to missions designed to image rocky exoplanets. To eliminate this large separation, the parabolic DM architecture makes the off-axis imaging elements in the optical train controllable. Simulations also show performance enhancements with the architecture change; larger bandwidths have been shown to be controllable with the parabolic DMs and the number of required actuators can be reduced. With a 32×32 pupil flat DM and two 16x16 parabolic DMs, we could obtain a 5 - 12 λ/D dark hole at 35% bandwidth. In addition to addressing the packaging challenge faced by future coronagraph missions, reducing the number of actuators reduces both cost and risk of having the entire coronagraph instrument's performance depend on two high-actuator count DMs. To test these simulations, Goddard is building a testbed and has a vendor developing the parabolic DM. Here we present these simulations, the current testbed performance, and the development plan to incorporate and test the parabolic DMs.

1. INTRODUCTION

To achieve the high level of contrast required to directly image exoplanets, coronagraphic instruments must have active wavefront control systems to estimate and compensate for aberrations of different temporal and spectral frequencies. The low-order wavefront sensor (LOWFS) estimates the dynamic aberrations such as line-of-sight (LoS) pointing errror and low-order aberrations such as focus, coma, spherical, and astigmatism. Algorithms such as speckle nulling,[2] electric field conjugation (EFC),[4] and stroke minimization[9] are used to calculate DM actuation to control quasi-static higher spatial frequency aberrations and dig the dark holes. The LoS pointing error is compensated by a tip/tilt mirror and a DM to cancel out the low-order aberrations. Conventionally, the dark hole digging techniques use two high actuator count flat DMs in the optical path, which results in any space mission having risk of single point failure. In addition to this risk, the minimum distance required between the DMs to effectively dig the dark holes for mission concepts such as LUVOIR is so long that it causes packaging issues with the existing rocket fairings. Groff et al.[5] showed that the parabolic mirrors used in the optical train could be made deformable with fewer actuator count than the flat DMs to reduce the risk of a space-based coronagraphic instrument by building redundancy into the DM control. This would also increase throughput by reducing the number of optical surfaces. By placing the control surfaces on the sources of aberrations themselves, it is possible to increase the control bandwidth too. We are working with vendors to manufacture off-axis parabolic DMs and building a lab to experimentally verify the concept. The lab is designed to be a multipurpose lab to experimentally verify different low and high-order wavefront control algorithms.

We will start Section 2 by describing the wavefront control using parabolic DMs. Section 3 presents the planned layout of the lab. In this section, we will describe the different elements of the testbed in detail. In Section 4, we will discuss the alignment of the proposed lab and then we conclude the paper in Section 5.

Further author information: (Send correspondence to Hari B. Subedi)
Email: hari.b.subedi@nasa.gov, Telephone: +13012865193

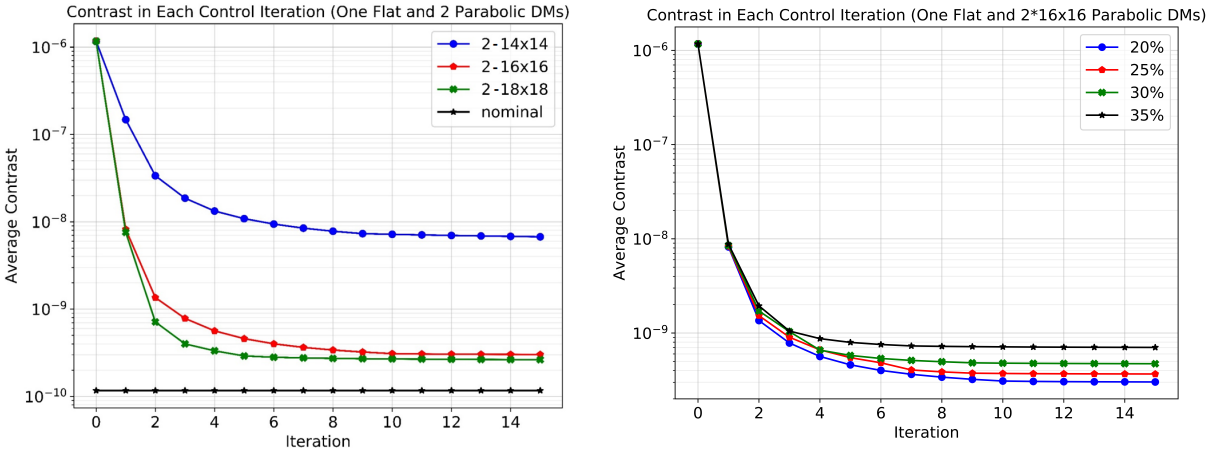

(a) Contrast vs iteration for different actuator count parabolic DMs.

(b) Contrast vs iteration for different bandwidths.

FIGURE 1: *Contrast curves*

2. WAVEFRONT CONTROL USING PARABOLIC DMS

Groff et al.[5] used a shaped pupil coronagraph (SPC)[6] ripple3 design to perform trade studies to determine the efficacy of using parabolic DMs for wavefront control. The study shows that 1) the full width half maximum (FWHM) of the actuator has a significant effect on the achievable contrast and 2) the minimum number of parabolic DM actuators required to achieve the desired high contrasts in broadband light is actually quite modest as long as there is one high actuator density DM at the pupil. Building on the results of this study, we performed further simulations to find the limits of using parabolic DMs for wavefront control. For the simulations presented in this section, we used the same SPC design but increased the size of the dark hole from $5-7.5\lambda/D$ to $5-12\lambda/D$. As we aim to determine the limits of the control achieved by the new DM architecture, we assume a perfect estimate of the wavefront and consider noiseless scenarios only. For the optimal DM command calculations, we use the EFC technique. We use the setup shown in Fig. 3 with a 32×32 Boston Micromachines (BMC) DM at the pupil access plane and two parabolic DMs - one as a focusing element and another as a collimating element as shown in the figure. The BMC DMs have a FWHM of 1.28 actuators and for the parabolic DMs we assume similar specifications like the ALPAO DM-97 which has the FWHM of 1.4 actuators.

First, we determine the number of actuators required to dig a high contrast two symmetric dark holes at 20% bandwidth with a central frequency of 635nm. We introduce phase and amplitude aberrations at the pupil plane and phase aberrations at the OAP surfaces. Due to these aberrations, the mean contrast in the dark holes degrades to 1.2×10^{-6} (Fig. 2a).

For this test, we use the 32×32 pupil access DM with two parabolic DMs (in focusing and collimating arrangement) each with 14×14, 16×16 or 18×18 actuators. From Fig. 2 a) it can be seen that using two 16×16 parabolic DMs improve the final contrast by more than an order of magnitude as compared to the setup with 14×14 DMs, but increasing the number of actuators to 18×18 has only a small improvement. We now test the improvement in the controllable bandwidth due to the parabolic DMs. For this test, we use same phase and amplitude aberrations as the actuator tests but change the bandwidth from 20% to 35% with an increment of 5%. For this test, we use two 16×16 parabolic DMs and a 32×32 BMC DM. The result of this test is presented in Fig. 2b) and Table 1. We can see that we can control the aberrations at 30% bandwidth to achieve similar final contrast level as compared to lower bandwidths.

3. LAB LAYOUT

To verify the performance of the parabolic DM architecture, we are building a testbed at NASA Goddard Space Flight Center. The layout of the proposed lab is shown in Fig. 3. A laser source will be used as a starlight

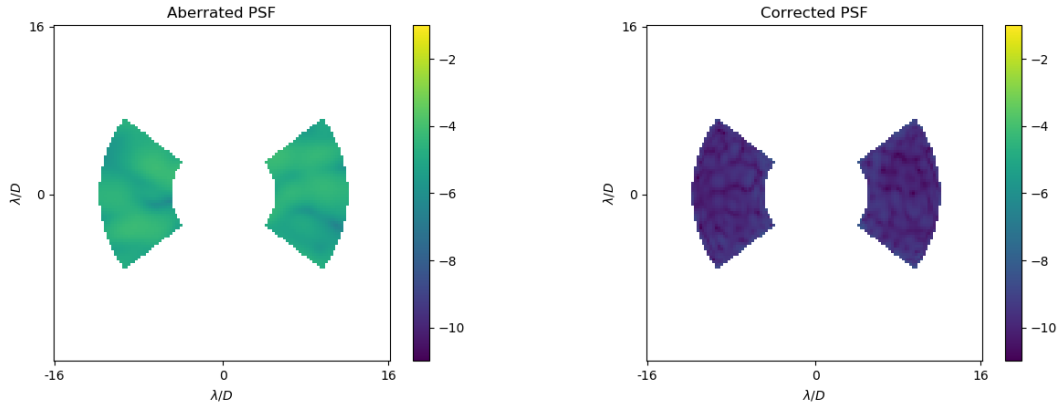

(a) Aberrated PSF due to phase and amplitude errors.

(b) Corrected PSF.

FIGURE 2: *PSF before and after wavefront control using a pupil DM and two 16×16 parabolic DMs. The simulations use 20% bandwidth light centered at 635nm.*

TABLE 1: *Final contrast for different bandwidths using two 16x16 parabolic DMs and one flat 32x32 pupil DM.*

Bandwidth	Final Contrast
20%	3.1e-10
25%	3.9e-10
30%	4.7e-10
35%	7.1e-10

emulator. The light from the source is collimated using an off-axis parabola (OAP) manufactured by Space Optics Research Lab (SORL). A Physic-Instruments (PI) tip-tilt stage with a 2-inch flat is placed at the first pupil. The focusing OAP after the tip-tilt mirror will be a deformable mirror OAP. By using mutiple SORL OAPs of different focal lengths, multiple pupil access planes are created. The BMC 32×32 actuator DM is placed at the next pupil plane. The next pupil plane has an apodizer and if required, a Lyot stop will be at another pupil plane. At the coronagraphic focal plane we have a Zernike phase mask. This mask directs the rejected starlight to the LOWFS camera and the remaining light to the science camera. Details of these optical elements are presented in the following section.

3.1 Apodizer

The apodizer shown in Fig. 4a) is a hard edge binary mask with the point spread function (PSF) as shown in Fig. 4b). The coronagraph has the average contrast of 10^{-8} over the dark zone (DZ) of $4\lambda/D - 12\lambda/D$, where λ is the wavelength and D is the diameter. We manufactured the apodizer by using a carbon nanotube technology at NASA Goddard Space Flight Center. Carbon nanotube is the darkest man-made material available. To manufacture a binary apodizer using this technology, the mirrors are fabricated from single crystal silicon which is figured flat. A multilayer coating resistant to 750C growth temperatures is applied as a reflective layer. The apodizer pattern is laser written on the mirror coating to a few microns resolution. The resist on the mirror is developed and an ultra-thin layer of catalyst applied. The residual catalyst is lifted from areas where no nanotube growth is desired, then the mirror is put in a tube furnace where carbon nanotubes are grown using a chemical vapor deposition process.

3.2 Focal Plane Mask/ Zernike Phase Mask

The focal plane mask (FPM) design is shown in Fig. 4c and the manufactured FPM is shown in Fig. 4f. The FPM has three different regions: 1) the reflective central phase disk of the FPM that has a diameter of $1.6\lambda/D$, 2) a reflective region outside the phase disk that has a radius of $4.5\lambda/D$, and 3) the outer bowtie shaped transparent

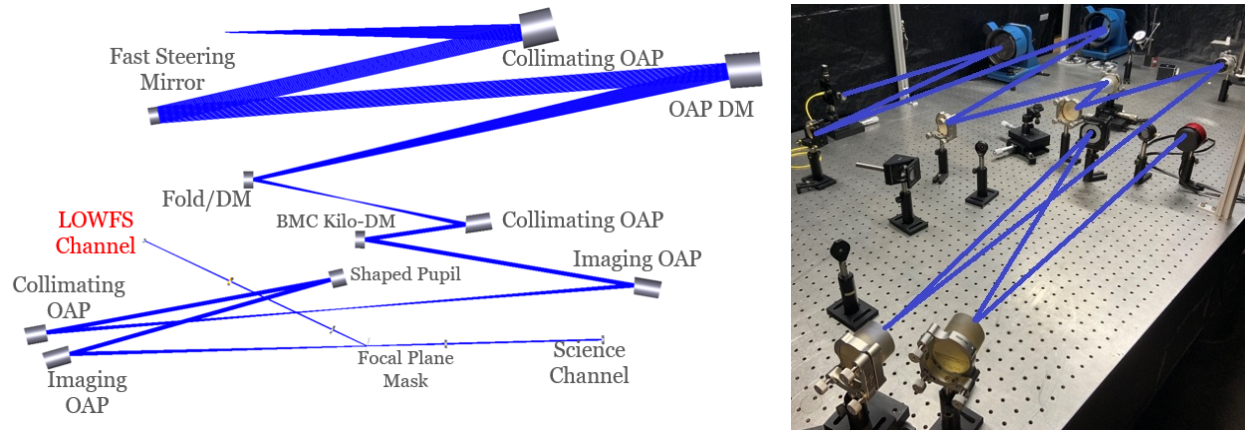

(a) Zemax drawing of the lab setup at NASA GSFC

(b) Aligned Lab setup at NASA GSFC

FIGURE 3: *a) Lab layout of the multipurpose lab being built at NASA GSFC. We intend to test different DM architectures and wavefront sensing and control techniques in this lab. In the long run, the setup will have two parabolic DMs and two flat DMs. The current setup has shaped pupil apodizer in the layout.*

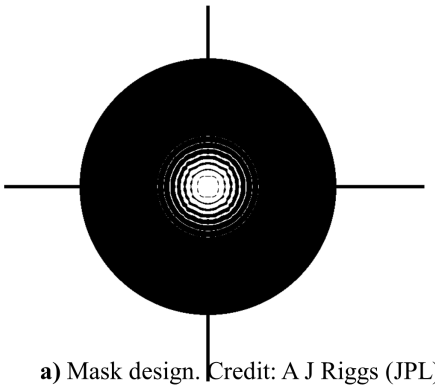

a) Mask design. Credit: A J Riggs (JPL)

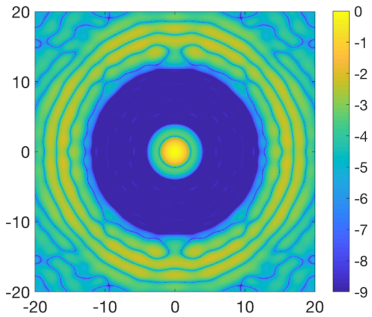

b) Simulated PSF with 4-12 λ/D annular dark hole

c) Focal plane mask design with bowtie through holes and a reflective central spot with a phase dimple for LOWFS

d) Carbon nanotube apodizer made by John Hagopian, Lambda Consulting

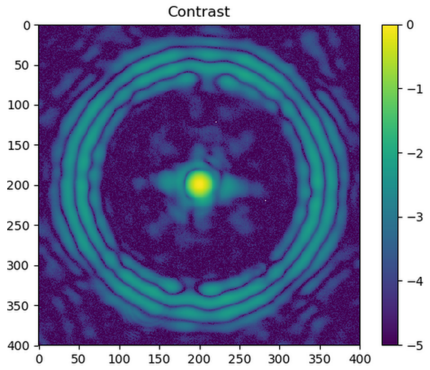

e) Lab PSF of the manufactured mask

f) Manufactured focal plane mask

FIGURE 4: *Mask designs and manufactured masks with the simulated PSF and the lab PSF*

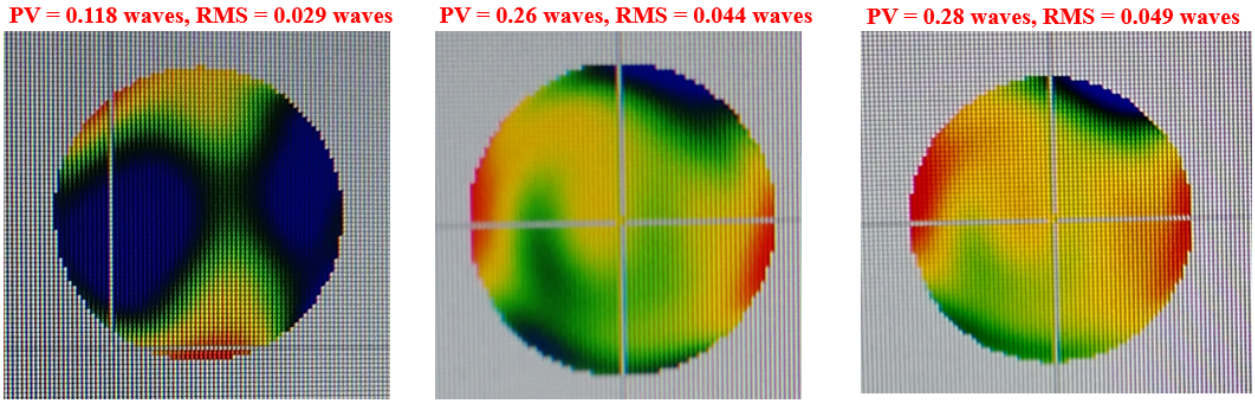

FIGURE 5: *Double pass wavefront aberrations measured at different pupil access planes. The first at the FSM location, second at the pupil access flat DM location, and the third at the SPC location.*

region from $4.5\lambda/D$ - $11.5\lambda/D$ at 150^o that lets light to the science path. The light that passes through the phase disk of the FPM acts as a reference wavefront and interferes with the light passing outside the phase disk which contains the information on wavefront aberrations. The interfered light is then relayed to another pupil plane, where the detector records the intensity pattern. This intensity pattern is related to the phase variation of the telescope pupil plane and depends on the size of the phase mask and the phase change introduced by this mask. Using the intensity pattern at the detector plane and the least-squares-fit algorithm, the low-order aberrations are inferred. This low-order wavefront sensor is called Zernike wavefront sensor.[1,3,7,8,10,11]

3.3 Parabolic Deformable Mirror

We are working with ALPAO in the manufacturing of two off-axis parabolic DMs to meet the following minimum specifications:

- Pitch: 3.1 mm
- Actuators : 277
- Effective Focal length: 1524mm
- Offset distance from the center: 254mm
- Resonant frequency: 500Hz
- Minimum frequency at phase lag of 45^o: 300Hz
- Maximum settling time (at +/-10%): 2ms
- Hysteresis: <10%
- Operating temperature: 25^o+/-5^oC
- Functional temperature: -5^oC to 45^oC
- OAP Shape accuracy < 30nm rms.

4. LABORATORY ALIGNMENT

To align the testbed we used a shearing interferometer for coarse alignment and a 4D Phasecam interferometer for fine alignment. The light from the interferometer was focused using a lens and the focus spot was used as a point source. The diverging light is collimated by the first OAP and a reflector is used in the beam path to reflect the light back to the interferometer for double pass interferometry. We changed the position, tip-tilt, and clocking of the OAP assembly to achieve phase aberrations of better than $\lambda/30$ RMS waves in double pass. We repeated the same procedure after placing each optic in the table based on the distances obtained from the Zemax model. The phase error at different relay pupil planes is shown in Fig. 5. The phase error is all these planes is less than $\lambda/20$ RMS waves in double pass. Fig. 4e) shows the first light PSF after the testbed alignment. We were able achieve a monochromatic contrast of 5×10^{-5} without active wavefront control.

5. CONCLUSION

Wavefront control is essential for any coronagraph-equipped direct imaging mission. Multiple deformable mirrors are used for wavefront control to achieve the required contrast. In simulation, we show that by making off-axis mirrors deformable we can control wavefront aberrations. In doing so, we are reducing the number of actuators required, thus reducing the cost and risk of failure. By using a 32×32 flat DM and two 16×16 parabolic DMs, we can achieve the high contrast and increase the controllable bandwidth. We are designing a lab to verify this new DM architecture and have provided required specifications to ALPAO to manufacture them. Most of the optical elements in the testbed are aligned with minimal alignment error.

6. ACKNOWLEDGEMENT

We would like to thank A J Riggs (JPL) for his contribution in mask design. The project is supported by NASA HQ directed ExoSpec work package.

REFERENCES

1. E. E. Bloemhof and J. K. Wallace. Phase contrast techniques for wavefront sensing and calibration in adaptive optics. In R. K. Tyson and M. Lloyd-Hart, editors, *Astronomical Adaptive Optics Systems and Applications*, volume 5169 of *Society of Photo-Optical Instrumentation Engineers (SPIE) Conference Series*, pages 309–320, December 2003.
2. P. J. Bordé and W. A. Traub. High-Contrast Imaging from Space: Speckle Nulling in a Low-Aberration Regime. *APJ*, 638:488–498, February 2006.
3. R. H. Dicke. Phase-contrast detection of telescope seeing errors and their correction. *APJ*, 198:605–615, June 1975.
4. A. Give'on, B. Kern, S. Shaklan, D. C. Moody, and L. Pueyo. Broadband wavefront correction algorithm for high-contrast imaging systems. In *Society of Photo-Optical Instrumentation Engineers (SPIE) Conference Series*, volume 6691 of *Society of Photo-Optical Instrumentation Engineers (SPIE) Conference Series*, September 2007.
5. Tyler D. Groff, Aaron Lemmer, and A. J. Eldorado Riggs. A new deformable mirror architecture for coronagraphic instrumentation. In Howard A. MacEwen, Giovanni G. Fazio, Makenzie Lystrup, Natalie Batalha, Nicholas Siegler, and Edward C. Tong, editors, *Space Telescopes and Instrumentation 2016: Optical, Infrared, and Millimeter Wave*, volume 9904, pages 697 – 704. International Society for Optics and Photonics, SPIE, 2016.
6. N. J. Kasdin, R. J. Vanderbei, D. N. Spergel, and M. G. Littman. Extrasolar Planet Finding via Optimal Apodized-Pupil and Shaped-Pupil Coronagraphs. *APJ*, 582:1147–1161, January 2003.
7. M. N'Diaye, K. Dohlen, T. Fusco, and B. Paul. Calibration of quasi-static aberrations in exoplanet direct-imaging instruments with a Zernike phase-mask sensor. *AAP*, 555:A94, July 2013.
8. Mamadou N'Diaye, Kjetil Dohlen, Amandine Caillat, Anne Costille, Thierry Fusco, Aïssa Jolivet, Fabrice Madec, Laurent Mugnier, Baptiste Paul, Jean-François Sauvage, Rémi Soummer, Arthur Vigan, and J. Kent Wallace. Design optimization and lab demonstration of ZELDA: a Zernike sensor for near-coronagraph quasi-static measurements. In Enrico Marchetti, Laird M. Close, and Jean-Pierre Véran, editors, *Adaptive Optics Systems IV*, volume 9148, pages 1775 – 1785. International Society for Optics and Photonics, SPIE, 2014.
9. L. Pueyo, J. Kay, N. J. Kasdin, T. Groff, M. Mc Elwain, A. Give'on, and R. Belikov. Optimal Dark Hole Generation via Two Deformable Mirrors with Stroke Minimization. *ArXiv e-prints*, November 2011.
10. F. Shi, K. Balasubramanian, R. Hein, R. Lam, D. Moore, J. Moore, K. Patterson, I. Poberezhskiy, J. Shields, E. Sidick, H. Tang, T. Truong, J. K. Wallace, X. Wang, and D. Wilson. Low-order wavefront sensing and control for WFIRST-AFTA coronagraph. *Journal of Astronomical Telescopes, Instruments, and Systems*, 2(1):011021, January 2016.
11. J. Kent Wallace, Shanti Rao, Rebecca M. Jensen-Clem, and Gene Serabyn. Phase-shifting zernike interferometer wavefront sensor. volume 8126, pages 81260F–81260F–11, 2011.